High power spiral cavity quantum cascade superluminescent emitter

Mei C. Zheng,[1*], Nyan L. Aung,[1] Abanti Basak,[1] Peter Q. Liu,[1,2] Xiaojun Wang,[3] Jen-Yu Fan,[3] Mariano Troccoli,[3] and Claire F. Gmachl[1]

[1]*Department of Electrical Engineering, Princeton University, Princeton, New Jersey 08544, USA*
[2]*Current address: Institute of Quantum Electronics, ETH Zürich, 8093, Zürich, Switzerland*
[3]*AdTech Optics Inc., City of Industry, California 91748, USA*
[*]*meizheng@princeton.edu*

Abstract: Quantum Cascade devices with an emission wavelength centered around 5 μm have been shaped into compact, yet long (8 mm and 12 mm) spiral cavities to increase mid-infrared superluminescence (SL) power. Up to ~57 mW of SL power at 250 K is obtained with a Gaussian emission spectrum with a full width at half maximum of 56 cm^{-1} and a coherence length of ~107 μm.

OCIS codes: (140.5965) Semiconductor lasers, quantum cascade; (140.3070) Infrared and far-infrared lasers.

References and links

1. K. Böhm, P. Marten, K. Petermann, E. Weidel, and R. Ulrich, "Low-drift fibre gyro using a superluminescent diode," Electron. Lett. **17**(10), 352–353 (1981).
2. A. Küng and P. Robert, "Measuring integrated optical circuits using a low-coherence light source," Opt. Eng. **34**(7), 2049–2054 (1995).
3. J. G. Fujimoto, C. Pitris, S. A. Boppart, and M. E. Brezinski, "Optical coherence tomography: an emerging technology for biomedical imaging and optical biopsy," Neoplasia **2**(1-2), 9–25 (2000).
4. A. B. Seddon, "Mid-infrared (IR) - A hot topic: The potential for using mid-IR light for non-invasive early detection of skin cancer in vivo," Phys. Status Solidi B **250**(5), 1020–1027 (2013).
5. C. S. Colley, J. C. Hebden, D. T. Delpy, A. D. Cambrey, R. A. Brown, E. A. Zibik, W. H. Ng, L. R. Wilson, and J. W. Cockburn, "Mid-infrared optical coherence tomography," Rev. Sci. Instrum. **78**(12), 123108 (2007).
6. R. Su, M. Kirillin, E. W. Chang, E. Sergeeva, S. H. Yun, and L. Mattsson, "Perspectives of mid-infrared optical coherence tomography for inspection and micrometrology of industrial ceramics," Opt. Express **22**(13), 15804–15819 (2014).
7. E. A. Zibik, W. H. Ng, D. G. Revin, L. R. Wilson, J. W. Cockburn, K. M. Groom, and M. Hopkinson, "Broadband 6 μm<λ< 8 μm superluminescent quantum cascade light-emitting diodes," Appl. Phys. Lett. **88**(12), 121109 (2006).
8. W. H. Ng, E. A. Zibik, M. R. Soulby, L. R. Wilson, J. W. Cockburn, H. Y. Liu, M. J. Steer, and M. Hopkinson, "Broadband quantum cascade laser emitting from 7.7 to 8.4 μm operating up to 340 K," J. Appl. Phys. **101**(4), 046103 (2007).
9. N. L. Aung, Z. Yu, Y. Yu, P. Q. Liu, X. Wang, J.-Y. Fan, M. Troccoli, and C. F. Gmachl, "High peak power (≥ 10 mW) quantum cascade superluminescent emitter," Appl. Phys. Lett. **105**(22), 221111 (2014).
10. J. D. Thomson, H. D. Summers, P. J. Hulyer, P. M. Smowton, and P. Blood, "Determination of single-pass optical gain and internal loss using a multisection device," Appl. Phys. Lett. **75**(17), 2527 (1999).
11. M. C. Zheng, P. Q. Liu, X. Wang, J.-Y. Fan, M. Troccoli, and C. F. Gmachl, "Wide single mode tuning in quantum cascade lasers with asymmetric Mach-Zehnder interferometer type cavities with separately biased arms," Appl. Phys. Lett. **103**(21), 211112 (2013).
12. S. Ahn, C. Schwarzer, T. Zederbauer, H. Detz, A. M. Andrews, W. Schrenk, and G. Strasser, "Enhanced light output power of quantum cascade lasers from a tilted front facet," Opt. Express **21**(13), 15869–15877 (2013).
13. P. Q. Liu, A. J. Hoffman, M. D. Escarra, K. J. Franz, J. B. Khurgin, Y. Dikmelik, X. Wang, J.-Y. Fan, and C. F. Gmachl, "Highly power-efficient quantum cascade lasers," Nat. Photonics **4**(2), 95–98 (2010).
14. A. F. Fercher, W. Drexler, C. K. Hitzenberger, and T. Lasser, "Optical coherence tomography – principles and applications," Rep. Prog. Phys. **66**(2), 239–303 (2003).

#229164 - $15.00 USD Received 4 Dec 2014; revised 22 Jan 2015; accepted 25 Jan 2015; published 30 Jan 2015

1. Introduction

Superluminescent light sources with low temporal and high spatial coherence have many industrial and medical applications [1–3]. In particular, such light sources in the near-infrared (near-IR) have been employed in optical coherence tomography (OCT) for high resolution and cross-sectional tomographic real time imaging of internal structures in the human eye [3]. Extending OCT to the mid-infrared (mid-IR) will potentially expand biomedical imaging to cancerous tissues [4] and compounds such as collagen amide, phosphate and carbonate, which have strong absorption spectra in the mid-IR [5]. Mid-IR OCT systems can also aid in industrial process monitoring [6]. However, due to a lack of an appropriate mid-IR superluminescent light source, such imaging systems in the mid-IR do not yet exist. Quantum cascade (QC) devices present themselves as potential superluminescent light sources in the mid-IR. However, it is challenging to achieve milliwatts of superluminescence (SL) power in QC devices due to low spontaneous emissions caused by the short non-radiative carrier lifetime of the intersubband transition. A peak optical power of 25 μW at 10 K was reported in [7] by replacing one mirror facet with a wet-etched facet in a 2 mm long Fabry-Perot cavity. Insufficient optical power prevents such sources from practical applications. While powerful broadband QC lasers exist [8], the long coherence length caused by lasing deteriorates image resolution in OCT systems [5].

Recently, a peak SL power of ~10 mW at 250 K was achieved by employing a round, wet-etched back facet with a Si_3N_4 anti-reflection coating and a 17° tilted cleaved front facet [9]. However, these emitters are 8 mm in length, which limits the compactness of these devices. This limitation constrains the realization of longer devices to generate higher SL power since the maximum attainable SL power increases approximately linearly with an increase in the device length [9].

In this work, we demonstrate a spiral cavity design, which is compact and enables the fabrication of longer devices without the need for greater chip area. Since our current supply limits room temperature operation of these devices, all measurements are performed from 80 K to 250 K. An output power of ~57 mW has been achieved with a 12 mm long spiral cavity at 250 K.

2. Spiral cavity design and fabrication

It has been shown [9,10] that the maximum amplified spontaneous emission (ASE) output intensity can be approximated as

$$I_{\max}(l) = T_f I_{spon} \frac{(e^C - 1)l}{C}, \tag{1}$$

where, $C = \frac{1}{2}\left(\ln\left(\frac{1}{R_f R_b} \right) \right)$, I_{spon} is the intensity of the spontaneous emission, l is the length of the cavity with a front and back facet reflectivity, R_f and R_b respectively, and T_f is the front facet transmissivity. Since the ASE output intensity is linearly proportional to the length of the cavity, l, longer devices will yield more power. In addition, the reflectivity of the back and front facets can be minimized to achieve the desired ASE output power. Spiral cavities with large bend radius (as opposed to linear cavities) can therefore facilitate more compact fabrication of longer devices.

The mid-IR superluminescent spiral cavity design is shown in Fig. 1(a). The spiral is connected to a rounded wet-etched facet at the inner end, and a 17° angled straight section with a cleaved facet at the outer end. The minimum spiral radius is chosen to be ~380 μm for negligible bending losses [11]. Two lengths of these cavities are fabricated, 8 mm and 12 mm. The lengths of the 17° angled straight ridges are ~950 μm for the 8 mm device and ~1325 μm

#229164 - $15.00 USD Received 4 Dec 2014; revised 22 Jan 2015; accepted 25 Jan 2015; published 30 Jan 2015

for the 12 mm device. Both of the waveguides are ~25 μm in width and ~6 μm in depth – deep enough to expose the active core while maintaining a slope at the etched back facet in the active region to reflect incident light into the substrate and to scatter the incident light with its curved wall. It is additionally coated with 1.2 μm of Si_3N_4 to further suppress the optical feedback from the back facet. The reflectivity of such a facet with the anti-reflection (AR) coating is experimentally determined to be ~10^{-5} by comparing the threshold current densities and independently measured net gain of two 4 mm long Fabry-Perot (FP) cavities – one with two cleaved facets and another with a cleaved front facet and a wet-etched, AR-coated back facet. The 17° angled ridge waveguide (as defined in Fig. 1(b)) serves to suppress the residual reflection from the front facets and has been reported to achieve a reflectivity of about ~10^{-2} [12].

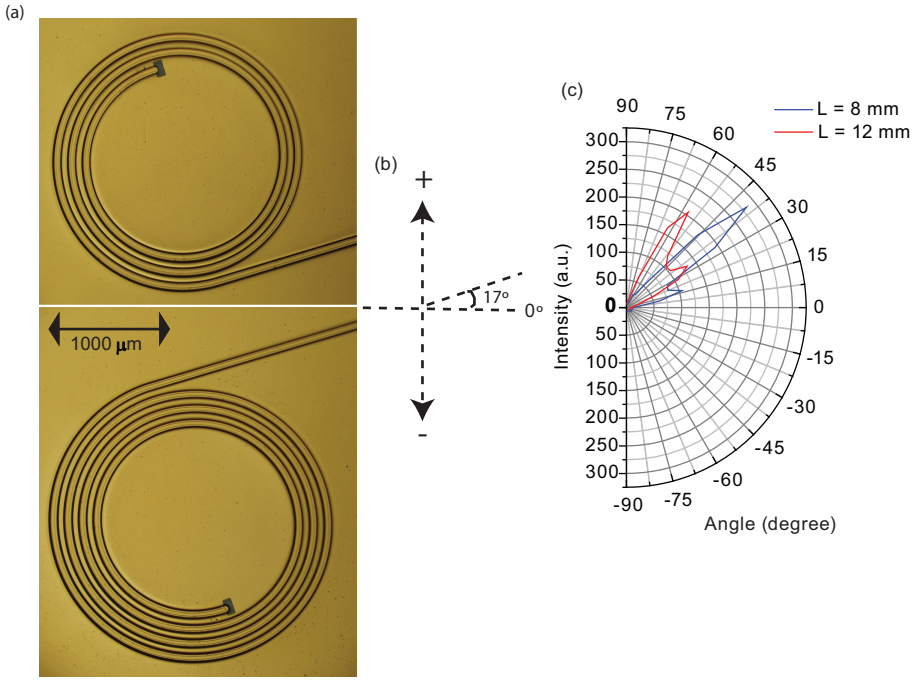

Fig. 1. (a) Optical microscope images of two spiral cavities with a total length of 8 mm (top) and 12 mm (bottom). (b) A schematic of the definition of positive and negative angles with respect to the 17° tilted front facet. (c) Far-field measurements taken at 80 K of the 8 mm device (blue) and the 12 mm device (red), both taken at ~2.6 A peak pulsed current.

The QC active core design employed in this work is based on an ultra-strong coupling scheme [9, 13], with an emission wavelength of ~5 μm at 80 K. The devices have been fabricated using standard ridge-laser processing: The waveguides are patterned by photolithography and wet-etched to ~6 μm deep; 1.2 μm of Si_3N_4 is deposited with plasma enhanced chemical vapor deposition (PECVD); contact windows of ~18 μm in width are opened at the top of the cavities (excluding the back facet) with photolithography and reactive-ion etching (RIE); contact patterns are again defined by photolithography and Ti/Au top metal contact of 30/300 nm is deposited through electron-beam evaporation from three different angles to ensure coverage on all sidewalls of the spiral shaped cavity. After lift-off, the substrate is thinned to ~200 μm and 20/200 nm of Ge/Au bottom metal contact is deposited through electron-beam evaporation. The devices are then mounted epitaxial side up to copper heat sinks.

#229164 - $15.00 USD Received 4 Dec 2014; revised 22 Jan 2015; accepted 25 Jan 2015; published 30 Jan 2015

3. Experimental results

Due to the tilted front facet, far-field measurements are taken to determine the angle of emission. The far-field measurements of both 8 mm and 12 mm devices, shown in Fig. 1(c) are taken below threshold at ~2.6 A at 80 K, with a liquid nitrogen cooled HgCdTe detector. Consistent with the previously reported devices [9], the light emission of both devices exhibit two peaks in the positive angle direction, with a full width at half maximum (FWHM) of ~15° and ~ 35° for 8 mm and 12 mm devices respectively. After rotating the devices to the angle that corresponds to their respective peak emission, light, current, and voltage (LIV) characterization of these devices are performed in pulsed mode with a current pulse width of

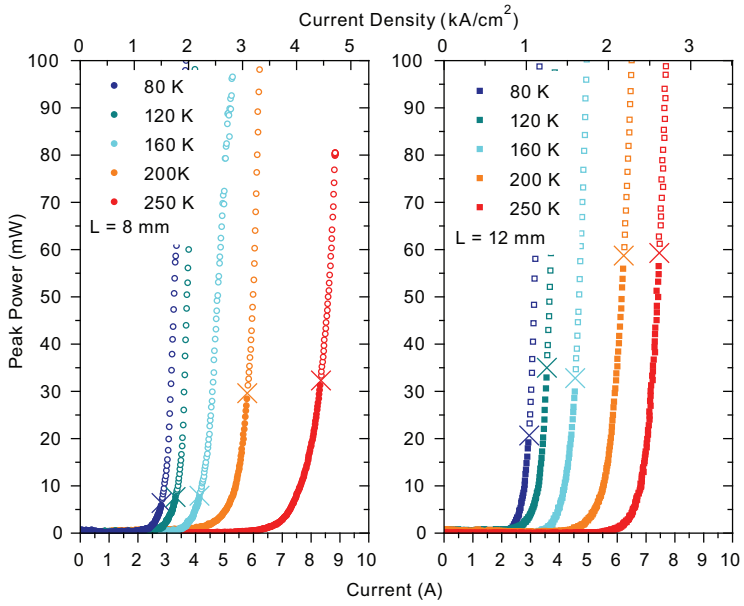

Fig. 2. Peak power vs. current taken under pulsed operation (100 ns pulse width at 5 kHz) across different temperatures for the 8 mm device (left, circles) and the 12 mm device (right, squares). The "X" marks the laser threshold. Close (open) symbols indicate the power below (above) threshold.

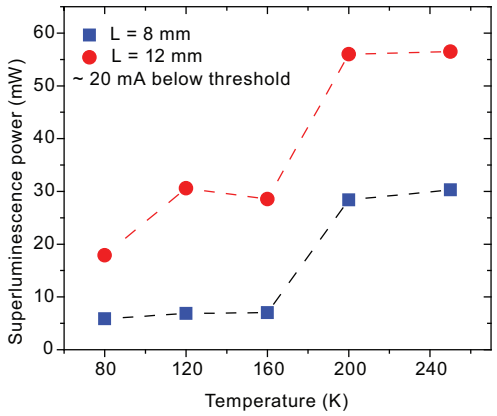

Fig. 3. Superluminescence power taken at ~20 mA below the laser threshold vs. temperature. Blue circles and red squares correspond to the 8 mm and 12 mm device, respectively. The dashed lines are a guide to the eye.

#229164 - $15.00 USD Received 4 Dec 2014; revised 22 Jan 2015; accepted 25 Jan 2015; published 30 Jan 2015

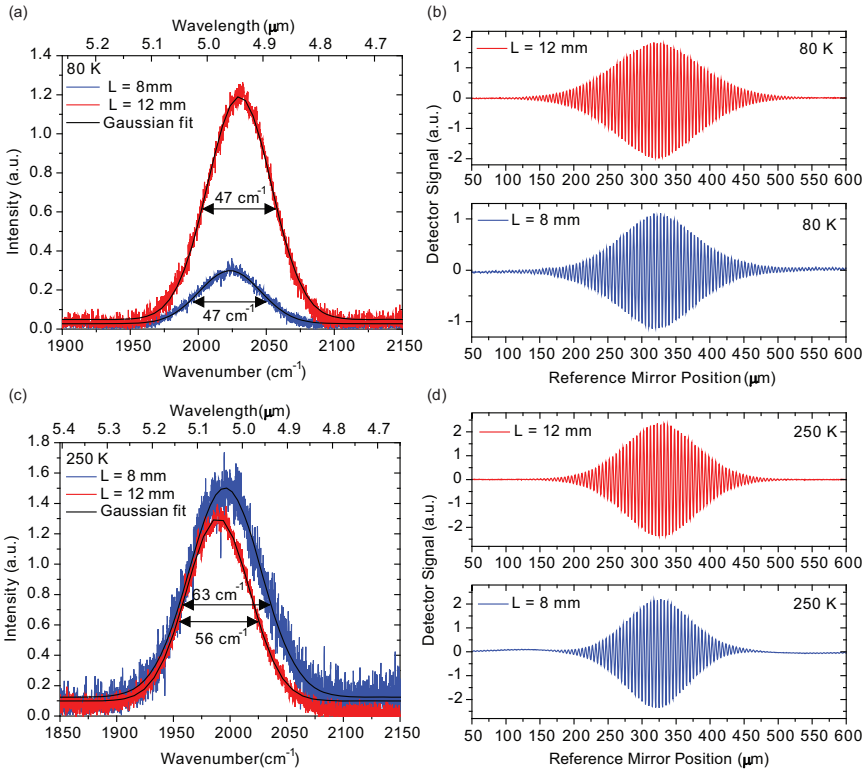

Fig. 4. (a) ASE spectra with a resolution of 0.125 cm^{-1} obtained in the fast scan mode of the FTIR of the 8 mm (blue) and 12 mm (red) devices at ~20 mA below threshold at 80 K. The black line corresponds to a Gaussian fit to the spectra. (b) The interferograms taken in step scan mode with a resolution of 16 cm^{-1} under the same operating conditions as the spectra shown in (a) of the 8 mm (blue) and 12 mm (red) devices. (c) ASE spectra taken under the same operating conditions and resolution as (a) at 250 K. The noisier spectrum in (c) would indicate that there is less power at 250 K, but the LI measurements indicate otherwise. (d) The interferograms taken under the same operating conditions and resolution as (b) at 250 K.) The offset in the Gaussian fit of (a) and (c) is due to the thermal background.

100 ns and a repetition rate of 5 kHz. Optical emission from the devices is collimated and focused onto a room temperature HgCdTe detector by a pair of ZnSe lenses. The LI characteristics of both devices across different temperatures are shown in Fig. 2, where the "X's" mark the lasing threshold, which are determined from their corresponding spectra. A representative 8 mm long device achieves > 5 mW of SL power across all temperatures before lasing. Above 200 K, ~30 mW of SL power is observed at ~20 mA below the lasing threshold. According to Eq. (1), a 12 mm device should outperform the 8 mm device by 50% due to the 50% increase in length. The best 12 mm device, in fact, emits significantly more power than the 8 mm one. It emits a SL power of > 20 mW across all temperatures. Above 200 K, ~57 mW of SL power is achieved at ~20 mA below lasing. Compared with the previously reported devices [9], the light emission in the spiral cavities exhibits a smoother transition from ASE to lasing. SL power obtained at ~20 mA below threshold was extracted for both devices at different temperatures and plotted in Fig. 3. Due to the increase in laser threshold with temperature, higher current is required to observe ASE at higher temperatures. Therefore, being beyond the technical limit of our current supply unit, SL power at temperatures above 250 K is not reported.

For potential imaging applications in OCT, the coherence length of the mid-IR source also plays an important role in addition to a high optical power emission. Since the coherence length determines the depth resolution of 3D images, a small coherence length is desired for

#229164 - $15.00 USD Received 4 Dec 2014; revised 22 Jan 2015; accepted 25 Jan 2015; published 30 Jan 2015

high quality imaging. For an ideal source with a broad Gaussian spectrum, the coherence length, l_c, is given by [14]

$$l_c = \frac{2\ln 2}{\pi}\frac{\bar{\lambda}^2}{\Delta\lambda} \tag{2}$$

where $\bar{\lambda}$ is the center wavelength and $\Delta\lambda$ is the FWHM. Therefore, at the longer wavelengths of the mid-IR region, the spectral width must increase significantly in order to maintain the same coherence length.

Emission spectra are taken with a Fourier Transform Infrared Spectrometer (FTIR) with 0.125 cm^{-1} resolution in the fast scan mode under the same operating condition as the characterization for the LIV to determine the laser threshold. The spectra taken at 80 K for both of the devices at ~20 mA below threshold are shown in Fig. 4 (a) and their corresponding interferograms taken in the step scan mode with a resolution of 16 cm^{-1} in Fig. 4 (b). Gaussian shaped spectra with FWHM of ~47 cm^{-1} are found for both devices at their maximum ASE power at 80 K. The smooth spectra are an indication that the emitter is indeed below threshold. The coherence length is determined from the interferograms to be ~112 μm and ~127 μm for the 8 mm and 12 mm long devices, respectively. Smaller coherence length is expected at higher temperature due to broadening in the ASE spectra. At 250 K, Gaussian shaped spectra (Fig. 4 (c)) with FWHM of 63 cm^{-1} and 56 cm^{-1} are observed for the 8 mm and 12 mm long devices, respectively, with a coherence length of ~94 μm and ~107 μm extracted from their corresponding interferograms (Fig. 4 (d)). The coherence length is also plotted as a function of peak power for the 12 mm long device at 200 K as shown in Fig. 5, where "X" indicates the lasing threshold. The increase in the coherence length with an increase in power is explained by the gain narrowing that occurs due to an increase in the pumping current. Overall, the coherence length revealed minor changes (~11 μm, ~10%) around threshold from an output power of ~20 mW to ~118 mW. Below threshold, from an emission power of ~20 mW to ~57 mW, the coherence length only increased by ~4 μm, making this a stable source for imaging materials that do not require finer than ~115 μm of depth resolution.

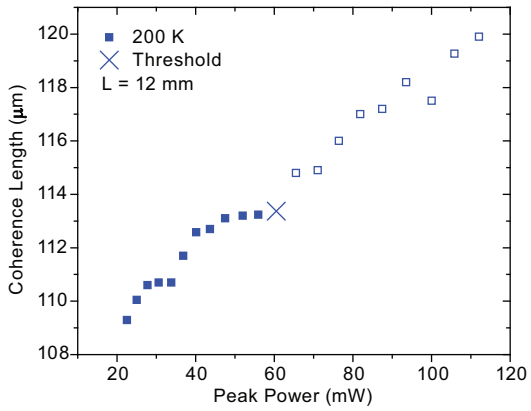

Fig. 5. Coherence length vs. peak power of the 12 mm device at 200 K. The "X" marks the laser threshold.

4. Conclusion

We have designed, fabricated, and demonstrated quantum cascade superluminescent emitters using spiral cavities joined to a 17° tilted ridge waveguides and wet-etched rounded back facets with a single layer of Si_3N_4 as anti-reflection coating. The devices that were

#229164 - $15.00 USD Received 4 Dec 2014; revised 22 Jan 2015; accepted 25 Jan 2015; published 30 Jan 2015

characterized are 8 mm or 12 mm in length. The emission spectra centered at ~5 μm for both types of devices are approximately Gaussian. The coherence lengths are determined from their corresponding interferograms to be ~94 μm and ~107 μm at 250 K for the 8 mm and 12 mm long devices, respectively. At these coherence lengths, the corresponding ASE peak power emitted are ~30 mW and ~57 mW, more than a threefold improvement from the previous result [9].

Acknowledgments

This work is support in part by MIRTHE (NSF-ERC # EEC-0540832). M. C. Zheng also acknowledges support from the NDSEG fellowship.

#229164 - $15.00 USD Received 4 Dec 2014; revised 22 Jan 2015; accepted 25 Jan 2015; published 30 Jan 2015